



CrossMark
click for updates

Cite this: *RSC Adv.*, 2015, 5, 36948

Natural kaolin derived stable SBA-15 as a support for Fe/BiOCl: a novel and efficient Fenton-like catalyst for the degradation of 2-nitrophenol†

Qihang Zhao, Xiaoyan Liu, Menglin Sun, Chunfang Du* and Zhiliang Liu*

The ordered mesoporous material SBA-15 (FCSBA-15) with an enhanced hydrothermal stability was successfully synthesized from natural kaolin in the presence of a fluorocarbon surfactant. FCSBA-15 was further used as the support for Fe/BiOCl with the aim of exploring its Fenton-like catalytic performance toward the degradation of 2-nitrophenol. Based on characterization techniques including X-ray diffraction (XRD), transmission electron microscopy (TEM) and high-resolution TEM (HRTEM), energy dispersive spectroscopy (EDS) and X-ray photoelectron spectroscopy (XPS), no phases referring to the Fe species were observed, suggesting that the Fe³⁺ ions may be present on the surface of flower-like BiOCl. It is noted that the Fe³⁺ ions could lead to a morphological reconstruction from BiOCl nanosheets to BiOCl flowers. The obtained Fe/BiOCl–FCSBA-15 exhibited an excellent degradation efficiency for 2-nitrophenol, which reached nearly 100% within 40 min by optimizing parameters such as the H₂O₂ dosage, pH value, temperature, Fe/Bi molar ratio and Bi/Si molar ratio. The finding reported here is important and may help to develop novel mesoporous matrix based systems for advanced catalysts.

Received 29th January 2015

Accepted 27th March 2015

DOI: 10.1039/c5ra01804h

www.rsc.org/advances

1. Introduction

Nitrophenols, widely used in the chemical industry for manufacturing, synthetic dyes, wood preservatives and pesticides, are common pollutants of wastewater and the environment and most of them have been included in the US Environmental Protection Agency (USEPA) list of priority pollutants.^{1–3} 2-Nitrophenol (2-NP) is one of the most bio-refractory, persistent, and highly toxic nitrophenols, the concentration of which is restricted by USEPA to less than 4.8 μg L⁻¹.^{4,5} Thus, the efficient control and degradation of 2-nitrophenol through a green and economic route is a most urgent task worldwide.

Many techniques have been proposed to treat hazardous 2-nitrophenol, including conventional biological oxidation,^{6,7} solvent extraction,⁸ thermal treatment and adsorption,^{9,10} *etc.* By comparison, catalytic wet peroxide oxidation (CWPO), an advanced oxidation process, is expectedly attractive due to its mild conditions, simple equipment and being environmentally friendly.¹¹ This process mostly involves some suitable catalyst, in particular iron based catalysts in the presence of hydrogen peroxide (H₂O₂), to improve the degradation of 2-nitrophenol through the formation of active hydroxyl radicals ([•]OH).¹²

Fe-involved homogeneous catalysis (Fenton reaction)^{13,14} and heterogeneous catalysis (Fenton-like reaction)^{15–17} have been extensively reported. Compared with homogeneous Fenton catalysis, the heterogeneous solid ion-based reaction is a highly promising alternative to expand the reaction conditions and prevent the precipitation of soluble iron and the accumulated iron sludge.^{18,19}

Fenton-like catalysis refers to the catalyst aggregation and difficult recycling from the solution. Therefore, catalysts are always loaded onto various supports, taking mesoporous matrices,^{20,21} clay minerals²² and zeolites^{23,24} as examples, for the purpose of retaining the nanostructure of the catalysts and easier recycling. SBA-15, an attractive mesoporous material due to its huge surface area, high pore volume, uniform pore size distribution, regular structure and higher thermal and hydrothermal stability than M41S materials,^{25,26} is often employed as the host matrix to participate in the catalysis process.^{27–29} The reagents used for synthesizing SBA-15 are mainly concentrated on tetramethylorthosilicate (TMOS),³⁰ tetraethylorthosilicate (TEOS)³¹ and water glass (Jo *et al.*),³² which are relatively expensive and hazardous to the environment. Available natural minerals, such as layered silicates rich with SiO₂ or Al₂O₃, would be more favorable raw starting materials for the preparation of mesoporous materials.^{33,34} Although many studies referring to the synthesis of ordered mesoporous materials, such as MCM-41 from kaolin, talc, bentonite, *etc.* have been reported,^{35–37} the relative work about SBA-15 being synthesized from natural minerals is limited.³⁸

College of Chemistry and Chemical Engineering, Inner Mongolia University, Hohhot, Inner Mongolia 010021, P. R. China. E-mail: cedchf@imu.edu.cn; cezlliu@imu.edu.cn; Fax: +86-471-4995414; Tel: +86-471-4995414

† Electronic supplementary information (ESI) available: Details of TEM images, EDS spectra, adsorption and degradation data of various samples. See DOI: 10.1039/c5ra01804h

In the present work, natural kaolin was chosen as a raw material to synthesize SBA-15 with an enhanced hydrothermal stability in the presence of a fluorocarbon surfactant (FSO-100). Furthermore, Fe³⁺ modified BiOCl particles loaded onto the SBA-15 was used as a heterogeneous green catalyst to degrade 2-nitrophenol in the presence of H₂O₂. Various reaction parameters, including H₂O₂ dosage, pH value, reaction temperature, Fe/Bi molar ratio and Bi/Si molar ratio were investigated.

2. Experimental

2.1 Materials

Natural kaolin from Maoming, China was used as a raw material to synthesize the mesoporous material FCSBA-15. The main chemical composition of the kaolin were as follows (wt%): SiO₂, 46.90; Al₂O₃, 37.80; MgO, 0.22; Fe₂O₃, 0.41; TiO₂, 0.25; CaO, 0.15; K₂O, 0.12; Na₂O, 0.18; and the loss on ignition was 14.00. Analytical grade chemicals of Bi(NO₃)₃·5H₂O, Fe(NO₃)₃·9H₂O, KCl, glycerol, NaOH, HCl were purchased from the Shanghai Chemical Industrial Co., Pluronic P123 was purchased from Sigma-Aldrich Co. and the fluorocarbon surfactant (FSO-100, F(CF₂CF₂)_mCH₂CH₂O(CH₂CH₂O)_nH, *m* = 1–7, *n* = 0–15) was purchased from DuPont Co., all of which were used as the starting materials without further purification.

2.2 Fluorocarbon surfactant assisted preparation of FCSBA-15 from kaolin

Kaolin was first treated at 850 °C to transform it into metakaolin, this was then leached with 6 M HCl at 80 °C for 4 h. The collected solid was washed with deionized water several times until the pH value of the washed water became about 7.0. The obtained solid was dried overnight and then calcined at 950 °C for 2 h again. This was then mixed with 5 M NaOH and hydrothermally treated in the conditions of 160 °C and 0.5 MPa for 3 h (solution A). The pH value of the obtained solution A was adjusted to 12.0 with 3 M HCl. The fluorocarbon surfactant FSO-100 and P123, with a molar ratio of FSO-100/P123 = 0.18, were mixed and dissolved in a solution of 25 mL HCl and 15 mL H₂O at 40 °C (solution B) for 30 h. After that, solution A was dropped into solution B and the mixture was transferred into a 100 mL Teflon-lined stainless steel autoclave and kept at 160 °C for 48 h. The resultant white product was filtered, washed several times with deionized water and ethanol, dried at 100 °C overnight, and then treated at 550 °C in air for 5 h. The final product was denoted as FCSBA-15. For comparison, the counterpart SBA-15 without the fluorocarbon surfactant was also prepared at 100 °C, the procedure used was the same as that of FCSBA-15 except for the addition of the fluorocarbon surfactant and hydrothermal temperature.

2.3 Synthesis of Fe/BiOCl loaded onto FCSBA-15 (Fe/BiOCl-FCSBA-15)

In a typical procedure, 0.776 g Bi(NO₃)₃·5H₂O and 0.129 g Fe(NO₃)₃·9H₂O were dissolved in 76 mL glycerol, denoted as solution I. Then, 0.12 g KCl was dissolved in 4 mL deionized water (solution II), which was subsequently poured into solution I and stirred. After stirring for 15 min, a certain amount of

FCSBA-15 was added into the solution and the mixture was then transferred into a 100 mL Teflon-lined stainless steel autoclave, heated up to 110 °C and kept at this temperature for 8 h. The resulting precipitate was collected by centrifugation, washed with ethanol and deionized water several times, then dried at 60 °C under vacuum and treated at 400 °C for 3 h with a heating rate of 3 °C min⁻¹. The final composite was marked as (y)Fe/BiOCl-FCSBA-15(x), where *x* and *y* indicate the molar ratio of BiOCl to FCSBA-15 and Fe to BiOCl, respectively.

2.4 Characterization

Detailed crystallographic information and evidence of the porous structures of the synthesized samples were obtained with an X-ray diffractometer (Empyrean Panalytical) with Cu K α radiation (λ = 0.15406 nm) over a scanning range of 2θ = 1–10° for small angle XRD (SAXRD) and 2θ = 10–80° for wide angle XRD (WAXRD). The detailed morphologies and structures of the samples were recorded by transmission electron microscopy (TEM) and high resolution TEM (HRTEM) on a JEM-2010 apparatus with an acceleration voltage of 200 kV. The surface states and chemical compositions of the samples were analyzed by X-ray photoelectron spectroscopy (XPS), which was carried out on a Thermo Escalab 250Xi with monochromatic Al K α radiation ($h\nu$ = 1486.6 eV). The specific surface areas (S_{BET}) of the samples were obtained from N₂ adsorption-desorption isotherms at 77 K (ASAP 2020). Prior to the sorption experiment, the materials were dehydrated by evacuation under specific conditions (200 °C, 10 h).

2.5 Degradation of 2-nitrophenol over Fe/BiOCl-FCSBA-15

The typical degradation procedure was as follows: 0.1 g of the prepared sample was added into 50 mL of 1×10^{-4} M 2-nitrophenol solution at 40–80 °C with a pH value of 2.0–6.0 adjusted by 0.1 M HCl. Then the homogeneous suspension was stirred for 20 min to ensure adsorption-desorption equilibrium. A certain amount of H₂O₂ was then added. At a given time interval, 3 mL of the suspension was taken out and then centrifuged for the subsequent concentration measurement. The 2-nitrophenol concentration was checked using a Hitachi U-3900 spectrophotometer.

3. Results and discussion

3.1 Characterization of FCSBA-15 and its hydrothermal stability

It is known that fluorocarbon surfactants are stable and can endure high temperatures (>200 °C), but they are not suitable as templates for the formation of ordered mesostructures due to the rigidity and strong hydrophobicity of the fluorocarbon chains.^{39,40} Expectably, the combination of a fluorocarbon surfactant and a hydrocarbon surfactant can induce various ordered mesoporous structures^{41,42} and improve the hydrothermal stability of the mesoporous materials,⁴³ which is helpful in Fenton-like reaction processes.

Fig. 1 shows the SAXRD patterns of FCSBA-15, SBA-15 and their counterparts after hydrothermal treatment. The

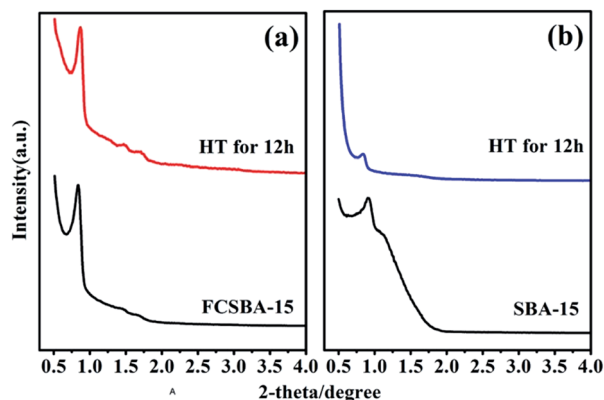


Fig. 1 SAXRD patterns of FCSBA-15 and SBA-15 before and after hydrothermal treatment.

hydrothermal treatment (HT) was done in a 100 mL Teflon-lined stainless steel autoclave at 100 °C for 12 h. As can be seen in Fig. 1, there is a distinct peak corresponding to the (100) plane of SBA-15 for the prepared products, with or without the fluorocarbon surfactant, which indicates that SBA-15 with an ordered mesostructure could be successfully synthesized from natural kaolin, even in the presence of the fluorocarbon surfactant FSO-100. After hydrothermal treatment, the peak intensity of the crystalline (100) plane for FCSBA-15 was maintained but it decreased for SBA-15, which implies that the prepared FCSBA-15 in the presence of the fluorocarbon surfactant displayed better hydrothermal stability than SBA-15 in the absence of the fluorocarbon surfactant.

To further investigate the porous properties of the synthesized samples, N₂ adsorption–desorption measurements were used to characterize the samples. The N₂ adsorption–desorption isotherms and pore size distributions of FCSBA-15 and SBA-15, as well as the counterparts after hydrothermal treatment, are shown in Fig. 2. As can be seen in Fig. 2, the shapes of the N₂ adsorption–desorption isotherms of FCSBA-15 and SBA-15 are typical IV type isotherms, corresponding to the standard mesoporous materials. The maximum pore size distributions were 6.2 nm and 3.9 nm for FCSBA-15 and SBA-15, respectively. After hydrothermal treatment, there was an obvious decrease in the N₂ adsorption amount for SBA-15 in comparison with FCSBA-15. Furthermore, the peak broadening in the pore size distribution curve confirms the collapse of the mesoporous structure of SBA-15 after hydrothermal treatment. The relative parameters of the porous properties for FCSBA-15 and SBA-15 before and after hydrothermal treatment are listed in Table 1. The maintained specific surface area and pore volume, as well as the average pore diameter, further confirm the improved hydrothermal stability of FCSBA-15 in contrast to SBA-15.

Fig. 3 presents TEM images of FCSBA-15 and SBA-15 before and after hydrothermal treatment. As shown in Fig. 3(a)–(c), both FCSBA-15 and SBA-15 exhibited well ordered mesostructures. After hydrothermal treatment for 12 h, the uniformly ordered mesostructure of FCSBA-15 remained (Fig. 3(b)) but it collapsed for SBA-15 (Fig. 3(d)). All of the information mentioned above indicates that FCSBA-15 exhibits higher

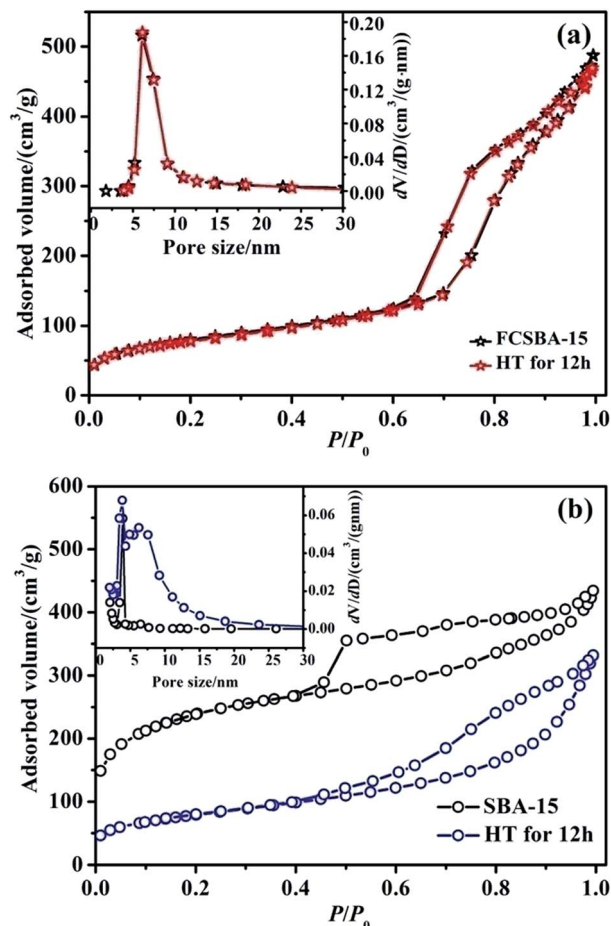


Fig. 2 N₂ adsorption–desorption isotherms and pore size distributions of FCSBA-15 and SBA-15 before and after hydrothermal treatment.

Table 1 The relative parameters of the porous properties of FCSBA-15 and SBA-15 before and after hydrothermal treatment^a

Samples	S_{BET} (m ² g ⁻¹)		Average pore diameter (nm)		Pore volume (cm ³ g ⁻¹)	
	HT _b	HT _a	HT _b	HT _a	HT _b	HT _a
FCSBA-15	281.3	272.4	8.7	8.5	0.69	0.68
SBA-15	787.3	276.0	4.1	6.9	0.62	0.44

^a HT_b values are before hydrothermal treatment and HT_a values are after hydrothermal treatment.

hydrothermal stability than SBA-15, which is expected to be beneficial for an application in a Fenton-like reaction process.

3.2 Characterization of catalyst Fe/BiOCl-FCSBA-15

Fig. 4 shows the XRD patterns of the Fe/BiOCl-FCSBA-15 catalysts with different Bi/Si and Fe/Bi molar ratios. All the diffraction peaks were in good agreement with those of the BiOCl standard (JCPDS 06-0249). The narrow sharp peaks suggest that the as-prepared catalysts are highly crystalline. The diffraction

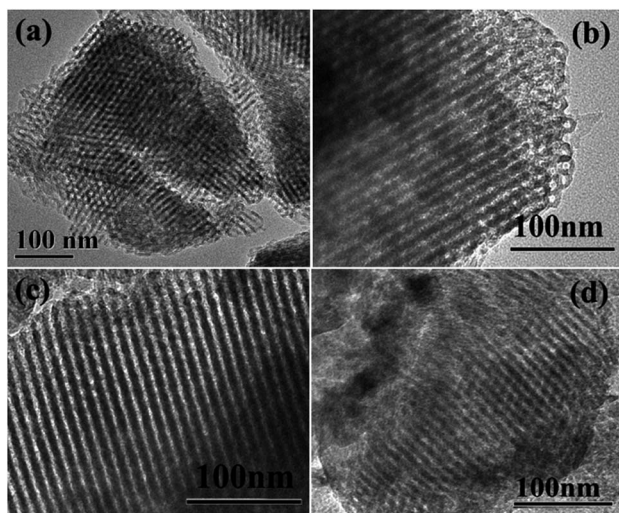


Fig. 3 TEM images of FCSBA-15 (a) and SBA-15 (b) and counterparts after hydrothermal treatment (c and d).

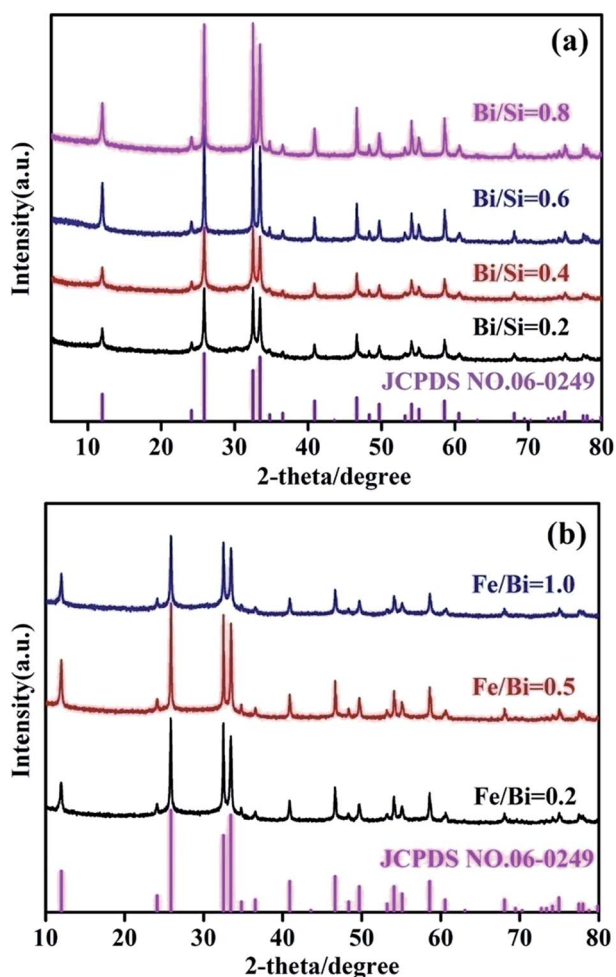


Fig. 4 XRD patterns of 0.5Fe/BiOCl-FCSBA-15 with different Bi/Si molar ratios (a) and Fe/BiOCl-SBA-15 (0.6) with different Fe/Bi molar ratios (b).

peaks of BiOCl in Fig. 4(a) become stronger with the increasing Bi/Si molar ratio. In Fig. 4(b), no diffraction peaks referring to iron species are observed, even when the Fe/Bi molar ratio reaches 1.0, which is in agreement with results of Cu-modified BiOCl.⁴⁴ In Cu-modified BiOCl, no typical patterns of copper species were observed even when the Cu/Bi molar ratio was 10 : 1, which was ascribed to the Cu ions being present on the surface of the BiOCl. Furthermore, no obvious peak shift is observed when increasing the Fe/Bi molar ratio in Fig. 4(b), implying that the Fe³⁺ ions were not doped into the lattice or substituted for Bi³⁺ ions in BiOCl.⁴⁵ Thus, it can be concluded that Fe³⁺ ions were present on the surface of the BiOCl.

The morphology and crystal structure of the catalyst 0.5Fe/BiOCl-FCSBA-15 (0.6) were obtained using the TEM technique. As shown in Fig. 5(a), Fe³⁺ ion modified BiOCl with a flower-like and nanosheet morphology was loaded onto mesoporous FCSBA-15. The EDS spectrum (Fig. 5(b)) reveals the co-presence of Fe, Bi, O, Cl and Si elements in the catalyst 0.5Fe/BiOCl-FCSBA-15 (0.6). The HRTEM image (Fig. 5(c)) is a magnified micrograph of part 1 (flower-like morphology) in Fig. 5(a), which clearly presents the lattice fringes of BiOCl with a *d* spacing of 0.276 nm, matching well with the (110) crystalline plane of BiOCl.

Fig. 5(d) shows the magnified micrograph of part 2 (nanosheet morphology) in Fig. 5(a), which also displays the distinct lattice fringes corresponding to the (110) crystalline plane of BiOCl. The selected area electron diffraction (SAED) pattern (inset in Fig. 5(d)) displays a spot pattern, suggesting a single-crystalline structure and it presents different crystalline planes of BiOCl of (110), (200) and (310). In comparison with pure BiOCl, which was composed of nanoplates displaying approximate round edges with a diameter of 50 nm and width of 10 nm, the Fe/BiOCl sample was mainly composed of hierarchical micro-flowers with a small number of square nanosheets (Fig. S1†). It has been reported that the introduction of Fe³⁺ ions

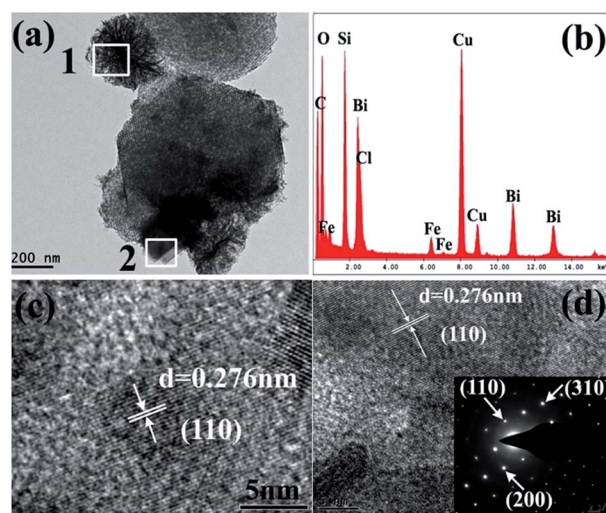


Fig. 5 TEM image (a), EDS spectrum (b) of catalyst 0.5Fe/BiOCl-FCSBA-15 (0.6) and magnified micrographs of part 1 (c) and part 2 (d) in (a). The inset in (d) is the SEAD pattern of part 2.

can induce a morphology transformation in bismuth oxyhalides.^{46,47} The results from the TEM images in our work indicate that the Fe^{3+} ions can induce the self-assembly of BiOCl nanosheets to form hierarchical micro-flowers. For Fe doped BiOBr, the morphology transformation was ascribed to the oriented attachment and Ostwald ripening.⁴⁶ The EDS spectrum indicates that there were only Bi, O, Cl and Si elements in the nanosheet Fe/BiOCl-FCSBA-15, but Fe, Bi, O, Cl and Si elements were present in the flower-like samples (Fig. S2†), which further suggests that the Fe modified BiOCl nanosheets were more favorable to assembling into flower-like structure.

To determine the surface composition and the chemical states of the elements, as well as to better understand the roles of the iron ions in Fenton-like catalytic oxidation, the catalyst 0.5Fe/BiOCl-FCSBA-15 (0.6) was studied by XPS (Fig. 6). The survey XPS spectrum indicates the co-presence of Bi, O, Cl, Fe, Si and C elements. The C peak was from the adventitious carbon on the surface of the sample. As shown in the high-resolution spectrum (Fig. 6(b)), the two strong peaks located at 164.7 eV and 159.4 eV are assigned to Bi 4f_{5/2} and Bi 4f_{7/2}, respectively,

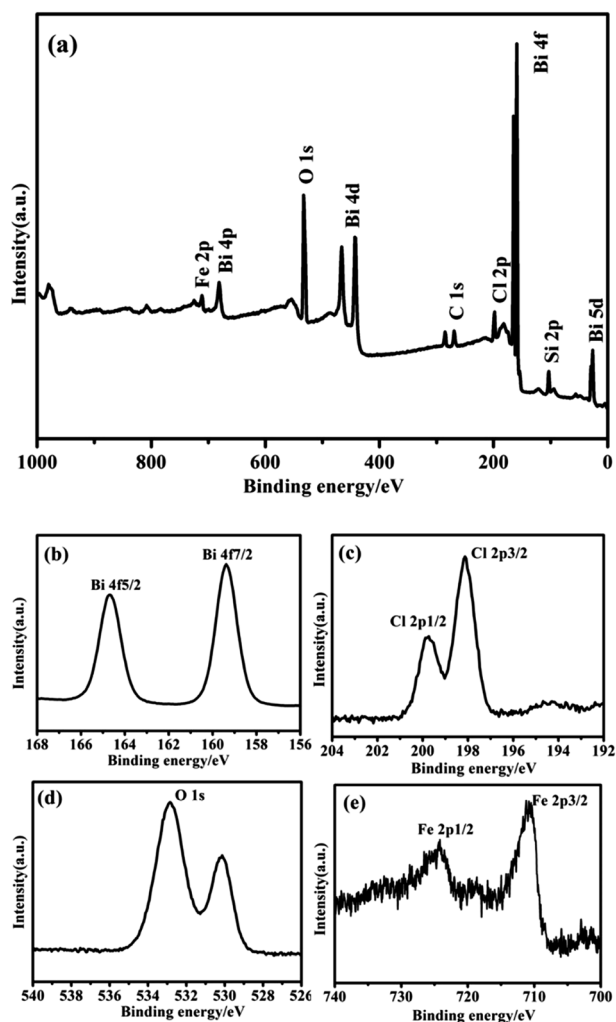


Fig. 6 XPS spectra of the catalyst 0.5Fe/BiOCl-FCSBA-15 (0.6): survey scan (a), Bi 4f (b), Cl 2p (c), O 1s (d), Fe 2p (e).

which is characteristic of the Bi^{3+} in the catalyst 0.5Fe/BiOCl-FCSBA-15 (0.6). In Fig. 6(c), there are two obvious peaks located at 198.1 eV and 199.8 eV, which are assigned to Cl 2p_{3/2} and Cl 2p_{1/2}, respectively. The high-resolution spectrum (Fig. 6(d)) shows that the binding energies of 532.8 eV and 530.2 eV correspond to O 1s, with the former assigned to the defect-oxide and hydroxyl-like groups⁴⁸ and the latter assigned to the lattice oxygen in Bi-O and Si-O bonds. As depicted in Fig. 6(e), the binding energies of Fe 2p were observed at 724.2 eV and 710.7 eV, which are assigned to Fe 2p_{1/2} and Fe 2p_{3/2} for Fe^{3+} , respectively. The contribution at around 720.0 eV belongs to the surface iron species and satellite signal of Fe^{3+} species.⁴⁹ The XPS technique was also used to determine the chemical composition. From the XPS data, the molar ratios of Fe/Bi and Bi/Si were estimated to be 0.36 and 0.57, respectively, which were close to the original molar ratios of Fe/Bi and Bi/Si.

Fig. 7 presents the N_2 adsorption-desorption isotherms of FCSBA-15 and 0.5Fe/BiOCl-FCSBA-15 with different amounts of BiOCl. As displayed in Fig. 7, no obvious shape change in the N_2 adsorption-desorption isotherm is observed when increasing the Bi/Si molar ratio. However, the N_2 adsorption amount, as well as S_{BET} , decreased when increasing the Bi/Si molar ratio. The S_{BET} value decreased from 247.9 $\text{m}^2 \text{g}^{-1}$ for FCSBA-15 to 115.6 $\text{m}^2 \text{g}^{-1}$ for 0.5Fe/BiOCl-FCSBA-15 with a Bi/Si molar ratio of 0.8. The decreased N_2 adsorption amount and S_{BET} value could be ascribed to the big particle size of the flower-like Fe/BiOCl, which greatly occupies the mesostructure of FCSBA-15 and thus inhibits the N_2 molecules from entering the mesochannels of the mesoporous material.

3.3 Evaluation of the degradation efficiency

The influence of various parameters, such as H_2O_2 dosage, pH value, degradation temperature, Fe/Bi molar ratio and Bi/Si molar ratio, on the degradation efficiency toward 2-nitrophenol are displayed in Fig. 8. Before the degradation process, the catalysts were immersed in the 2-nitrophenol solution for 20 min to ensure an adsorption-desorption equilibrium. It is

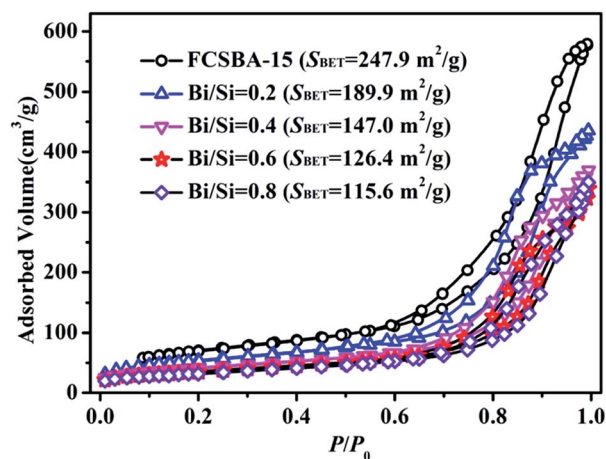


Fig. 7 N_2 adsorption-desorption isotherms of 0.5Fe/BiOCl-FCSBA-15 with different Bi/Si molar ratios.

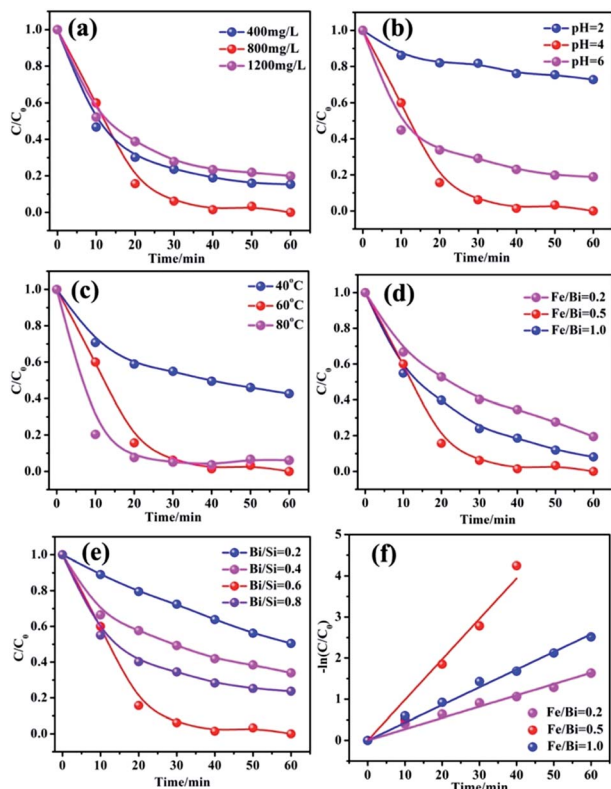


Fig. 8 Effects of various variables on 2-nitrophenol degradation by the catalyst Fe/BiOCl-FCSBA-15; (a) effect of H_2O_2 dosage ($T = 60\text{ }^\circ\text{C}$, $\text{pH} = 4$, Fe/Bi molar ratio = 0.5, Bi/Si molar ratio = 0.6); (b) effect of pH value ($T = 60\text{ }^\circ\text{C}$, H_2O_2 dosage = 800 mg L^{-1} , Fe/Bi molar ratio = 0.5, Bi/Si molar ratio = 0.6); (c) effect of degradation temperature ($\text{pH} = 4$, H_2O_2 dosage = 800 mg L^{-1} , Fe/Bi molar ratio = 0.5, Bi/Si molar ratio = 0.6); (d) effect of Fe/Bi molar ratio ($T = 60\text{ }^\circ\text{C}$, $\text{pH} = 4$, H_2O_2 dosage = 800 mg L^{-1} , Bi/Si molar ratio = 0.6); (e) effect of Bi/Si molar ratio ($T = 60\text{ }^\circ\text{C}$, $\text{pH} = 4$, H_2O_2 dosage = 800 mg L^{-1} , Fe/Bi molar ratio = 0.5); (f) determination of reaction rate constants in the degradation of 2-nitrophenol over the catalyst Fe/BiOCl-FCSBA-15 with different Fe/Bi molar ratios ($T = 60\text{ }^\circ\text{C}$, $\text{pH} = 4$, H_2O_2 dosage = 800 mg L^{-1} , Bi/Si molar ratio = 0.6).

seen that the Fe/BiOCl-FCSBA-15 catalyst showed no apparent adsorption toward 2-nitrophenol (Fig. S3†). It is well known that H_2O_2 plays a vital role in the degradation of dyes with Fenton and Fenton-like reactions.⁵⁰ Thus, the influence of the H_2O_2 dosage on the degradation of 2-nitrophenol was investigated. As shown in Fig. 8(a), the degradation efficiency was improved when increasing the amount of H_2O_2 , whereas the degradation efficiency obviously decreased with an excessive H_2O_2 dosage of 1200 mg L^{-1} . At a lower concentration of H_2O_2 , there are only a small number of $\cdot\text{OH}$ radicals produced. So the limited $\cdot\text{OH}$ cannot initiate and finish the degradation reaction rapidly and completely. When increasing the amount of H_2O_2 to more than 800 mg L^{-1} , the extra H_2O_2 would be a powerful scavenger which reacts with $\cdot\text{OH}$ to generate $\text{HO}_2\cdot$, O_2 or H_2O :^{50,51}



The generated $\text{HO}_2\cdot$ are much less reactive and have no contribution to the degradation reaction, which causes the

lower degradation rate.⁵² Thus, a reasonable concentration of H_2O_2 is indispensable for Fenton and Fenton-like reactions. The degradation efficiency for 2-nitrophenol can reach nearly 100% within 40 min over the catalyst $0.5\text{Fe}/\text{BiOCl-FCSBA-15}$ (0.6) with the concentration of H_2O_2 being 800 mg L^{-1} . For comparison, the degradation reaction with H_2O_2 in the absence of the catalyst was also conducted (Fig. S4†), the result of which showed that the 2-nitrophenol solution is relatively stable in the presence of H_2O_2 without the catalyst Fe/BiOCl-SBA-15 and the degradation efficiency only reaches about 30%. Thus, the co-presence of H_2O_2 and the catalyst enhances the degradation efficiency for 2-nitrophenol.

Fig. 8(b) displays the effect of the pH value on the degradation efficiency toward 2-nitrophenol over the catalyst Fe/BiOCl-FCSBA-15. It has been reported that an acid environment is favorable for generating the maximum amount of $\cdot\text{OH}$, which is helpful for the Fenton-like reaction.⁵³ Thus, the adopted range of pH values for the degradation of 2-nitrophenol was between 2 and 6. As shown in Fig. 8(b), the degradation rate of 2-nitrophenol is optimal at a pH value of 4. Furthermore, the degradation efficiency can reach 81% even in weak acid conditions ($\text{pH} = 6$). It also can be observed that the strong acid environment does not facilitate the degradation reaction. This phenomenon is attributed to the easy decomposition of H_2O_2 , which is due to the scavenging of $\cdot\text{OH}$ by H^+ ions to form O_2 and H_2O ⁵¹ or the scavenger effect of Cl^- on $\cdot\text{OH}$.⁵⁴

The degradation of 2-nitrophenol over the catalyst Fe/BiOCl-FCSBA-15 was also studied by varying the degradation temperature from $40\text{ }^\circ\text{C}$ to $80\text{ }^\circ\text{C}$, which is plotted in Fig. 8(c). As depicted in Fig. 8(c), the degradation rate increased with raising the temperature. At $40\text{ }^\circ\text{C}$, a fifty percent degradation efficiency was observed and at $60\text{ }^\circ\text{C}$, nearly 100% degradation efficiency was obtained within 40 min. It has been reported that an elevation of temperature can accelerate the generation of $\cdot\text{OH}$, which indicates that there would be less H_2O_2 available for scavenging the $\cdot\text{OH}$. At a temperature of $40\text{ }^\circ\text{C}$, the lower degradation efficiency was ascribed to the slow generation of $\cdot\text{OH}$,⁵¹ and the higher degradation efficiency at $60\text{ }^\circ\text{C}$ may be due to the faster production of $\cdot\text{OH}$. After the temperature reaches $80\text{ }^\circ\text{C}$, the degradation efficiency was not enhanced dramatically, but the degradation rate was improved dramatically, which was in accordance with the results of Inchaurredo.⁵⁴

The optimization study for the Fe dosage amount was carried out by varying the Fe/Bi molar ratio from 0.2 to 1.0, which is presented in Fig. 8(d). It can be observed that the maximum 2-nitrophenol degradation efficiency was achieved with a Fe/Bi molar ratio of 0.5, and the degradation efficiency decreased with both an increase and a decrease from the Fe/Bi molar ratio of 0.5. The increased availability of active sites for the generation of radicals is responsible for the enhanced degradation efficiency, and the decomposition of H_2O_2 , caused by the high catalytic activity of the extra catalyst, may be the reason for the decreased degradation efficiency. Furthermore, Zhan⁵⁵ proposed that in the conditions of a high catalyst dosage, the $\cdot\text{OH}$ may react immediately with the intermediate compounds

produced from dye degradation, which can result in the reduced utilization of H_2O_2 for the further degradation of dyes.

The influence of the BiOCl dosage on the 2-nitrophenol degradation efficiency was evaluated by changing the Bi/Si molar ratio over the range of 0.2 to 0.8. As indicated in Fig. 8(e), the degradation rate accelerated first and then slowed down when increasing the BiOCl amount, reaching a maximum efficiency with the Bi/Si molar ratio at 0.6. For comparison, the catalyst Fe/FCSBA-15 without BiOCl was also synthesized and the catalytic properties for 2-nitrophenol degradation were also studied (Fig. S5†). As shown in Fig. S5,† the degradation efficiency of the catalyst Fe/BiOCl-FCSBA-15 was higher than that of the catalyst Fe/FCSBA-15. Thus, it is concluded that the degradation efficiency of 2-nitrophenol is greatly improved by BiOCl. To further confirm the role of BiOCl in the 2-nitrophenol degradation process, both pure BiOCl and Bi_2O_3 were synthesized and their degradation behavior toward 2-nitrophenol were also checked (Fig. S6†). It can be seen that both BiOCl and Bi_2O_3 show a degradation efficiency toward 2-nitrophenol, which may be ascribed to Bi ions. In addition, the pure Fe/BiOCl catalyst without the matrix FCSBA-15 was also prepared and its catalytic behaviour for 2-nitrophenol degradation is displayed in Fig. S7.† The degradation results suggest that the catalyst Fe/BiOCl loaded onto FCSBA-15 shows a better catalytic performance than pure Fe/BiOCl, indicating that the porous matrix has an important role in the Fenton-like reaction. Considering these results, it can be concluded that the catalyst Fe/BiOCl-FCSBA-15 with a Fe/Bi molar ratio of 0.5 and a Bi/Si molar ratio of 0.6, with degradation conditions of H_2O_2 dosage = 800 mg L^{-1} , pH value = 4.0 and $T = 60 \text{ }^\circ\text{C}$, displays the best degradation efficiency toward 2-nitrophenol, which reached nearly 100% within 40 min.

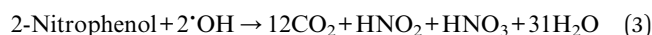
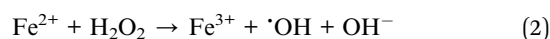
The 2-nitrophenol concentration *versus* the reaction time was further analysed using the equation for pseudo-first-order kinetics $\ln(C/C_0) = -kt$, where C_0 and C are the 2-nitrophenol concentration in the solution at time $t = 0$ and t , respectively, and k is the pseudo-first-order rate constant. The degradation rates of 2-nitrophenol over the Fe/BiOCl-FCSBA-15 (0.6) catalysts with different Fe/Bi molar ratios are displayed in Fig. 8(f). The degradation rates as influenced by the other parameters, including H_2O_2 dosage, pH value, degradation temperature and Bi/Si molar ratio are shown in Fig. S8.† The related calculated degradation constants k are listed in Table S1.† As shown in Fig. 8(f), S8 and Table S1,† the catalyst 0.5Fe/BiOCl-FCSBA-15 (0.6) in oxidation conditions of H_2O_2 dosage = 800 mg L^{-1} , pH = 4 and $T = 60 \text{ }^\circ\text{C}$ (consideration of energy consumption) showed the fastest degradation rate of $9.85 \times 10^{-2} \text{ min}^{-1}$.

To check the structural stability of the synthesized catalysts, the XRD pattern of the catalyst 0.5Fe/BiOCl-FCSBA-15 (0.6) after the degradation of 2-nitrophenol was measured, and is shown in Fig. S9.† It can be observed that there are no obvious peak changes between the XRD patterns of the catalyst before and after the degradation process, which indicates the structural stability of the synthesized catalysts. Furthermore, the reusability of the catalyst 0.5Fe/BiOCl-FCSBA-15 (0.6) was also investigated. However, the result was not ideal and needs to be further improved (Fig. S10†), which may be related to the Fe^{3+} ions leaching into the solution. As described in Fig. 4, the Fe^{3+}

ions are present on the surface of BiOCl, just like Cu-modified BiOCl,⁴⁴ which indicates that the Fe^{3+} ions do not exist in a crystalline state, therefore they are very unstable and favorable to be leached into the solution.

3.4 Possible mechanism for the degradation of 2-nitrophenol

It has been proposed that for heterogeneous Fenton-like reactions, the Fe ions form complexes with peroxide species and this is then followed by steps of dissociation reactions to generate $\cdot\text{OH}$, which plays a vital role in the Fenton-like oxidation process.⁵² The possible mechanism for hydroxyl radical generation by Fe/BiOCl-FCSBA-15 is given in Fig. 9. Generally, under acidic or neutral conditions, a complex between Fe^{3+} and H_2O_2 is formed through H_2O_2 activation by the catalysts.⁵⁶ The complex subsequently converts to Fe^{2+} and $\text{HO}_2\cdot$, and the generated $\text{HO}_2\cdot$ further reacts with Fe^{3+} to produce Fe^{2+} . Then, all the produced Fe^{2+} reacts with H_2O_2 to generate the $\cdot\text{OH}$, which is prepared for participating in the degradation process of 2-nitrophenol. The possible reactions involved can be summarized as eqn (1)–(3).



Moreover, the presence of Bi ions was also favorable for the degradation efficiency of 2-nitrophenol, and thus the combined effect of the Fe ions and Bi ions is responsible for the excellent degradation efficiency for the catalyst Fe/BiOCl-FCSBA-15 on 2-nitrophenol.

To further evaluate the important role of $\cdot\text{OH}$, various scavengers including isopropanol (IPA) and methanol (MeOH) were used (Fig. 10). As shown in Fig. 10, large decreases are seen in the degradation efficiency for 2-nitrophenol, from nearly 100 to 20 and 30% after adding IPA and MeOH, respectively. The results strongly suggest that a large number of $\cdot\text{OH}$ radicals are generated in the oxidation process, which have a prominent role in the degradation of 2-nitrophenol.

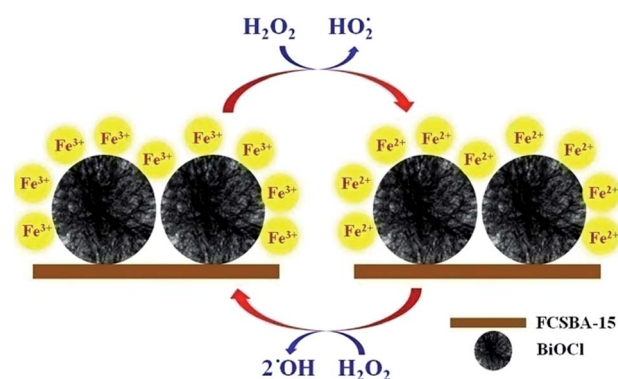


Fig. 9 Hydroxyl radical generation mechanism.

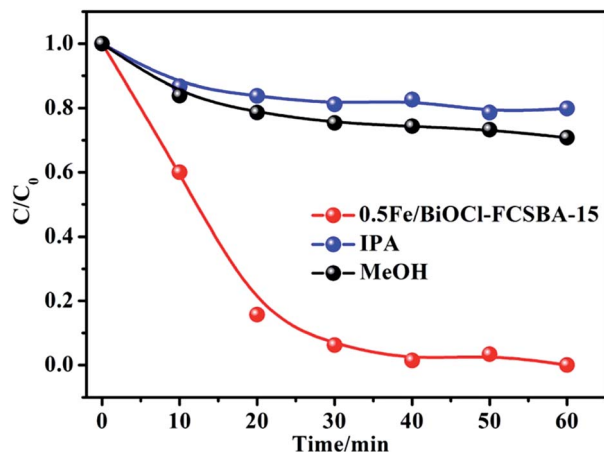


Fig. 10 Effects of IPA and MeOH on the degradation of 2-nitrophenol over the catalyst 0.5Fe/BiOCl-FCSBA-15 (0.6) ($T = 60\text{ }^{\circ}\text{C}$, $\text{pH} = 4$, H_2O_2 dosage = 800 mg L^{-1} , IPA = 0.26 mol L^{-1} , MeOH = 0.048 mol L^{-1}).

4. Conclusions

Natural kaolin was used as raw material to synthesize the ordered mesoporous material SBA-15 (FCSBA-15) the assistance of fluorocarbon surfactant. The material showed a specific surface area (S_{BET}) of $247.9\text{ m}^2\text{ g}^{-1}$, a pore volume of $0.69\text{ m}^3\text{ g}^{-1}$ and a maximum pore size distribution of 6.2 nm. The synthesized FCSBA-15 displayed an enhanced hydrothermal stability over SBA-15 without the fluorocarbon surfactant, which is beneficial for the following Fenton-like reaction. FCSBA-15 loaded Fe^{3+} modified BiOCl particles (Fe/BiOCl-FCSBA-15) were also synthesized. The results indicated that the presence of Fe^{3+} could induce the nanosheet BiOCl to self-assemble into flower-like BiOCl. The obtained catalyst Fe/BiOCl-FCSBA-15 exhibited an excellent degradation efficiency for 2-nitrophenol, which can reach nearly 100% within 40 min in the optimum conditions of H_2O_2 dosage = 800 mg L^{-1} , $\text{pH} = 4$, $T = 60\text{ }^{\circ}\text{C}$, Fe/Bi molar ratio = 0.5 and Bi/Si molar ratio = 0.6.

Acknowledgements

This work was supported by the National Natural Science Foundation of China (NSFC, no. 51102129 and 51462025) and the Inner Mongolia Provincial Natural Science Foundation of China (no. 2013MS0204).

Notes and references

- Ö. Aktaş and F. Çeçen, *J. Hazard. Mater.*, 2010, **177**, 956.
- M. B. Cassidy, H. Lee, J. T. Trevors and R. B. Zablutowicz, *J. Ind. Microbiol. Biotechnol.*, 1999, **23**, 232.
- B. R. Zaidi, S. H. Imam and R. V. Greene, *Curr. Microbiol.*, 1996, **33**, 292.
- N. Oturan, M. Hamza, S. Ammar, R. Abdelhédi and M. A. Oturan, *J. Electroanal. Chem.*, 2011, **661**, 66.
- E. Lipczynska-Kochany, *Chemosphere*, 1991, **22**, 529.
- S. Chaliha and K. G. Bhattacharyya, *Ind. Eng. Chem. Res.*, 2008, **47**, 1370.
- R. A. Kristanti, T. Toyama, T. Hadibarata, Y. Tanaka and K. Mori, *RSC Adv.*, 2014, **4**, 1616.
- R. A. Doong, R. A. Maithreepala and S.-M. Chang, *Water Sci. Technol.*, 2000, **42**, 253.
- W. F. Jardim, S. G. Moraes and M. M. K. Takiyama, *Water Res.*, 1997, **31**, 1728.
- T. G. Danis, T. A. Albanis, D. E. Petrakis and P. J. Promonis, *Water Res.*, 1998, **32**, 295.
- C. W. Jones, *Applications of Hydrogen Peroxide and Derivatives*, The Royal Society of Chemistry, Cambridge, UK, 1999.
- R. S. Ribeiro, A. M. T. Silva, J. L. Figueiredo, J. L. Faria and H. T. Gomes, *Appl. Catal., B*, 2013, **140–141**, 356.
- W. Zhu, J. Zhang, H. Li, Y. Chao, W. Jiang, S. Yin and H. Liu, *RSC Adv.*, 2012, **2**, 658.
- P. V. Nidheesh and R. Gandhimathi, *RSC Adv.*, 2014, **4**, 27946.
- S.-T. Yang, W. Zhang, J. Xie, R. Liao, X. Zhang, B. Yu, R. Wu, X. Liu, H. Liu and Z. Guo, *RSC Adv.*, 2015, **5**, 5458.
- N. N. Tušar, D. Maučec, M. Rangus, I. Arčon, M. Mazaj, M. Cotman, A. Pintar and V. Kaučič, *Adv. Funct. Mater.*, 2012, **22**, 820.
- X. Zhang, Y. Chen, N. Zhao, H. Liu and Y. Wei, *RSC Adv.*, 2014, **4**, 21575.
- L. J. Xu and J. L. Wang, *Environ. Sci. Technol.*, 2012, **46**, 10145.
- H. Lim, J. Lee, S. M. Jin, J. Kim, J. Yoon and T. Hyeon, *Chem. Commun.*, 2006, 463.
- P. Xiao, H. Li, T. Wang, X. Xu, J. Lin and J. Zhu, *RSC Adv.*, 2014, **4**, 12601.
- Y.-P. Zhu, T.-Z. Ren and Z. Y. Yuan, *RSC Adv.*, 2015, **5**, 7628.
- Z. Huang, P. Wu, H. Li, Y. Zhu and N. Zhu, *RSC Adv.*, 2014, **4**, 6500.
- R. Gonzalez-Olmos, F.-D. Kopinke, K. Mackenzie and A. Georgi, *Environ. Sci. Technol.*, 2013, **47**, 2353.
- Y. Hu, Y. Zhang and Y. Tang, *RSC Adv.*, 2012, **2**, 6036.
- D. Zhao, Q. Huo, J. Feng, B. F. Chmelka and G. D. Stucky, *J. Am. Chem. Soc.*, 1998, **120**, 6024.
- D. Zhao, J. Feng, Q. Huo, N. Melosh, G. H. Fredrickson, B. F. Chmelka and G. D. Stucky, *Science*, 1998, **279**, 548.
- J. Ma, J. Chu, L. Qiang and J. Xue, *RSC Adv.*, 2012, **2**, 3753.
- S. Sareen, V. Mutreja, S. Singh and B. Pai, *RSC Adv.*, 2015, **5**, 184.
- T. Tsoncheva, M. Järn, D. Paneva, M. Dimitrov and I. Mitov, *Microporous Mesoporous Mater.*, 2011, **137**, 56.
- L. Cao and M. Kruk, *Colloids Surf., A*, 2010, **357**, 91.
- Y. Ding, H. Dan and X. Lu, *Mater. Chem. Phys.*, 2014, **148**, 1.
- C. Jo, K. Kim and R. Ryoo, *Microporous Mesoporous Mater.*, 2009, **124**, 45.
- Y. Xie, Y. Zhang, J. Ouyang and H. Yang, *Phys. Chem. Miner.*, 2014, **41**, 497.
- J. Jin, J. Ouyang and H. Yang, *Appl. Clay Sci.*, 2014, **99**, 246.
- C. Du and H. Yang, *J. Colloid Interface Sci.*, 2012, **369**, 216.
- H. Yang, C. Du, S. Jin, A. Tang and G. Li, *Microporous Mesoporous Mater.*, 2007, **102**, 204.

- 37 H. Yang, Y. Deng, C. Du and S. Jin, *Appl. Clay Sci.*, 2010, **47**, 351.
- 38 G. M. Paula, L. A. Lima and M. G. F. Rodrigues, *Mater. Sci. Forum*, 2014, **798–799**, 116.
- 39 Y. Muto, K. Esumi, K. Meguro and R. Zana, *J. Colloid Interface Sci.*, 1987, **120**, 162.
- 40 F. S. Xiao, *Angew. Chem., Int. Ed.*, 2003, **42**, 3633.
- 41 Y. Han and J. Y. Ying, *Angew. Chem., Int. Ed.*, 2005, **117**, 292.
- 42 J. Liu, S. Z. Qiao, S. B. Hartono and G. Q. Lu, *Angew. Chem., Int. Ed.*, 2010, **49**, 4981.
- 43 Y. Han, D. Li, L. Zhao, J. Song, X. Yang, N. Li, C. Li, S. Wu, X. Xu, X. Meng, K. Lin and F. S. Xiao, *Angew. Chem., Int. Ed.*, 2003, **42**, 3633.
- 44 J. Di, J. Xia, S. Yin, H. Xu, L. Xu, Y. Xu, M. He and H. Li, *RSC Adv.*, 2014, **4**, 14281.
- 45 N. Li, X. Hua, K. Wang, Y. Jin, J. Xu, M. Chen and F. Teng, *Dalton Trans.*, 2014, **43**, 13742.
- 46 G. Jiang, X. Wang, Z. Wei, X. Li, X. Xi, R. Hu, B. Tang, R. Wang, S. Wang, T. Wang and X. Chen, *J. Mater. Chem. A*, 2013, **1**, 2406.
- 47 Z. Liu, B. Wu, Y. Zhu, D. Yin and L. Wang, *Catal. Lett.*, 2012, **142**, 1489.
- 48 Z. Mei, Y. Li, M. Fan, L. Zhao and J. Zhao, *Chem. Eng. J.*, 2015, **259**, 293.
- 49 G. Zhang, L. Qin, Y. Wu, Z. Xu and X. Guo, *Nanoscale*, 2015, **7**, 1102.
- 50 M. Wang, Z. Shu, L. Zhang, X. Fan, G. Tao, Y. Wang, L. Chen, M. Wu and J. Shi, *Dalton Trans.*, 2014, **43**, 9234.
- 51 V. Subbaramaiah, V. C. Srivastava and I. D. Mall, *Ind. Eng. Chem. Res.*, 2013, **52**, 9021.
- 52 P. Shukla, S. Wang, H. Sun, H.-M. Ang and M. Tadé, *Chem. Eng. J.*, 2010, **164**, 255.
- 53 S. M. Arnold, W. Jhickey and R. F. Harris, *Sci. Technol.*, 1995, **29**, 2083.
- 54 N. S. Inchaurredo, P. Massa, R. Fenoglio, J. Font and P. Haure, *Chem. Eng. J.*, 2012, **198–199**, 426.
- 55 Y. Zhan, X. Zhou, B. Fu and Y. Chen, *J. Hazard. Mater.*, 2011, **187**, 348.
- 56 W. Luo, L. Zhu, N. Wang, H. Tang, M. Cao and Y. She, *Environ. Sci. Technol.*, 2010, **44**, 1786.